

# High-pressure study of azurite $\text{Cu}_3(\text{CO}_3)_2(\text{OH})_2$ by synchrotron radiation X-ray diffraction and Raman spectroscopy

Jingui Xu<sup>1,2</sup> · Yunqian Kuang<sup>1,2</sup> · Bo Zhang<sup>1,2</sup> · Yonggang Liu<sup>1</sup> · Dawei Fan<sup>1,3</sup> · Wenge Zhou<sup>1</sup> · Hongsen Xie<sup>1</sup>

HPSTAR  
152-2015

Received: 21 December 2014 / Accepted: 1 July 2015  
© Springer-Verlag Berlin Heidelberg 2015

**Abstract** The high-pressure properties of natural azurite [ $\text{Cu}_3(\text{CO}_3)_2(\text{OH})_2$ ] have been investigated by in situ synchrotron powder X-ray diffraction and Raman spectroscopy up to 11 and 16 GPa at room temperature, respectively. The results indicate that azurite is stable within the pressure region in this study. The pressure–volume data from in situ X-ray diffraction experiments were described by a third-order Birch–Murnaghan equation of state with  $V_0 = 304.5$  (4)  $\text{Å}^3$ ,  $K_0 = 40$  (2) GPa and  $K_0' = 5.5$  (6). The  $K_0$  was obtained as 45.1 (8) GPa when  $K_0'$  was fixed at 4. The axial compressional behavior of azurite was also fitted with a linearized third-order Birch–Murnaghan equation of state, showing an intense anisotropy with  $K_{a0} = 29.7$  (9) GPa,  $K_{b0} = 25.0$  (7) GPa and  $K_{c0} = 280$  (55) GPa. In addition, the Raman spectroscopy of azurite in this study also presents the weak  $[\text{OH}]^-$  group and the rigid  $[\text{CO}_3]^{2-}$  group. The different high-pressure behaviors of azurite and malachite combined with the smaller isothermal bulk modulus compared with certain anhydrous carbonates and the obvious compression anisotropy of azurite were discussed with the experimental results in this study together with the results from previous studies. Furthermore, the effect of hydroxyl on the high-pressure behaviors of carbonates was also discussed.

**Keywords** Azurite · High pressure · Synchrotron X-ray diffraction · Raman spectroscopy · Diamond anvil cell

## Introduction

Carbonates are the main carbon-bearing phases on the Earth's surface, and they can be transported to the Earth's mantle along with oceanic lithosphere (Seto et al. 2008). In addition, they are considered to be the potential hosts of carbon in the mantle because of the low solubility of carbon in the silicates of the mantle (Kepler et al. 2003; Dasgupta et al. 2013). The existences of carbonate minerals at the mineral inclusions in natural diamonds from the lower part of the transition zone and lower mantle (Brenker et al. 2007; Logvinova et al. 2008; Wang et al. 1996) imply that carbonates (such as magnesite, dolomite and Ba–Sr carbonate) can be stable at the mantle depth. Therefore, studies on the behaviors of carbonate minerals at high-temperature and high-pressure conditions are important to understand the Earth's global carbon cycle. The extensive investigations of carbonates at extreme conditions are also aroused by the fact that the presence of carbon has strong effects on the physical and chemical properties of the Earth's interior (e.g., Gaillard et al. 2008; Dasgupta and Hirschmann 2010; Jana and Walker 1997).

Laboratory studies of carbonate minerals at high pressure and high temperature mainly focus on magnesite [ $\text{MgCO}_3$ ] and calcite [ $\text{CaCO}_3$ ] because these are the most dominant carbonates in the deep Earth (Oganov et al. 2006; Gao et al. 2014a). High-pressure and high-temperature experiments on magnesite [ $\text{MgCO}_3$ ] show its stability at the depth of the Earth's lower mantle (Isshiki et al. 2004; Oganov et al. 2008), and thus, it is considered to be a likely host of carbon in Earth's interior. Differently,

✉ Dawei Fan  
fandawei1982@126.com

<sup>1</sup> Key Laboratory of High-Temperature and High-Pressure Laboratory for High Temperature and High Pressure Study of the Earth's Interior, Institute of Geochemistry, Chinese Academy of Sciences, Guiyang 550002, China

<sup>2</sup> University of Chinese Academy of Sciences, Beijing 100049, China

<sup>3</sup> Center for High Pressure Science and Technology Advanced Research, Changchun 130012, China

calcite [ $\text{CaCO}_3$ ] undergoes several pressure-induced phase transitions to aragonite at upper mantle conditions (e.g., Suito et al. 2001). Similar to calcite, dolomite [(Ca, Mg)  $\text{CO}_3$ ] is also not stable with pressure and breaks down into a denser magnesite and aragonite [ $\text{CaCO}_3$ ] at about 7 GPa (Martinez et al. 1996; Buob et al. 2006). If minor Fe is added into structure of dolomite, however, it can be stable at the pressure and temperature conditions of Earth's deep mantle (Mao et al. 2011). Additionally, a number of high-pressure and high-temperature studies (e.g., Litasov et al. 2013; Boulard et al. 2012) focus on siderite [ $\text{FeCO}_3$ ] due to its presence in natural diamond (Stachel et al. 2000), indicating that it is also a candidate of carbon host in the deep Earth. Other carbonate minerals (e.g.,  $\text{PbCO}_3$ ,  $\text{BaCO}_3$ ) whose structural phase transitions may occur at more accessible P–T condition ranges are also studied at extreme conditions (Ono et al. 2008; Minch et al. 2010a). The study results of these carbonate minerals can be used to deduce the structural information of the important carbonates such as magnesite at high pressures. These studied carbonate minerals include [ $\text{ZnCO}_3$ ] (Gao et al. 2014b), rhodochrosite [ $\text{MnCO}_3$ ] (Ono 2007a), cerussite [ $\text{PbCO}_3$ ] (Minch et al. 2010a), witherite [ $\text{BaCO}_3$ ] (Townsend et al. 2013; Ono 2007b; Chaney et al. 2014) and otavite [ $\text{CdCO}_3$ ] (Liu and Lin 1997), etc.

Although most of the carbonates have been extensively investigated at high-pressure and high-temperature conditions, researches on the effect of hydroxyl on high-pressure properties of carbonates are still limited (Merlini et al. 2012). As a kind of hydrous carbonate, azurite [ $\text{Cu}_3(\text{CO}_3)_2(\text{OH})_2$ ] can be a proper sample to understand the effect of hydrogen on the behaviors of carbonates at extreme conditions. Azurite [ $\text{Cu}_3(\text{CO}_3)_2(\text{OH})_2$ ] is a hydrous copper carbonate and also one of the two basic copper carbonate minerals, the other being malachite [ $\text{Cu}_2(\text{OH})_2\text{CO}_3$ ]. Generally, azurite has a relationship of intergrowth with malachite [ $\text{Cu}_2(\text{OH})_2\text{CO}_3$ ] in the upper oxidized zone of copper ore deposits (Anthony et al. 1995). Gattow and Zemann (1958) first determined the crystal structure of azurite, and whereafter the crystal structure of azurite was refined by Zigan and Schuster (1972) using single-crystal neutron diffraction data as well as Belokoneva et al. (2001) with single-crystal X-ray diffraction data. Anhydrous carbonates can be classified into three types based on their structure differences: calcite group, aragonite group and dolomite group (Klein et al. 1993). Calcite group is trigonal with space group  $R\bar{3}c$ , aragonite group has orthorhombic structures ( $Pmcn$ ), and dolomite group is also trigonal like calcite group but with lower symmetry ( $R\bar{3}$ ). Unlike anhydrous carbonates, azurite belongs to monoclinic crystal system, and its space group is  $P2_1/c$ . Lately, Rule et al. (2011) presented their single-crystal neutron diffraction results of azurite, drawing the conclusion that the crystal structure

of azurite can be described with the space group  $P2_1$ , but this difference has no great influence on lattice parameters and atomic fractional coordinates. In the crystal structure of azurite, a triangle is formed by three oxygen ions surrounding one carbon ion; the copper ions are connected to four oxygen ions forming squares (Fig. 1). There are two kinds of coordination of the Cu ions: The Cu(1) ions are coordinated by O(1) and O(2) ions, whereas the remaining Cu ions (Cu(2)) are coordinated with O(1), O(3) and O(4) ions (Fig. 1a). Frost et al. (2002), Mattei et al. (2008) and Buzgar and Apopei (2009) well assigned the Raman bands of azurite to the corresponding vibrational groups. These investigations presented that the Raman spectrum of azurite is composed of three types of modes: [ $\text{CO}_3$ ] $^{2-}$  groups (internal modes), [ $\text{OH}$ ] $^-$  groups and the Cu–O vibrational modes (external or lattice modes).

To date, however, much of our knowledge about azurite comes from the studies at ambient conditions, and the knowledge of the high-pressure properties of hydrous copper carbonates is very limited (Merlini et al. 2012). Therefore, in the present paper, we investigated the compressional behavior of natural azurite at room temperature and high pressure in a diamond anvil cell, using in situ angle-dispersive X-ray synchrotron powder diffraction and Raman spectroscopy. The results are then used to probe the effect of hydrogen on the behaviors of carbonates at extreme conditions.

## Experiments

The natural azurite sample was collected from Yunnan Province, China. The pure azurite mineral grains were selected by hand under a microscope and then ground under ethanol in an agate mortar for 4–6 h. The ground samples were examined using the conventional powder X-ray diffraction method with a D/Max-2200 X-ray diffractometer equipped with graphite crystal monochromator and Cu  $K\alpha$  radiation, after being heated at 50 °C in a constant temperature furnace for 2 h. The ambient X-ray spectrum of azurite was indexed according to the standard spectra (JCPDS72-1270), confirming that the structure of the natural azurite mineral was monoclinic and belongs to the  $P2_1/c$  space group.

*In situ* high-pressure angle-dispersive X-ray diffraction experiments were performed at the BL15U1 beamline, Shanghai Synchrotron Radiation Facility (SSRF) and 4W2 beamline of Beijing Synchrotron Radiation Facility (BSRF). The incident synchrotron X-ray beam was monochromatic with a wavelength of 0.6199 Å. A symmetric diamond anvil cell (DAC) equipped with two diamonds anvils (500- $\mu\text{m}$ -diameter culet) and tungsten carbide supports was used to generate the high pressure. A rhenium

**Fig. 1** Crystal structure of azurite  $\text{Cu}_3(\text{CO}_3)_2(\text{OH})_2$  (a), calcite type (b) and aragonite type (c) at ambient pressure and room temperature

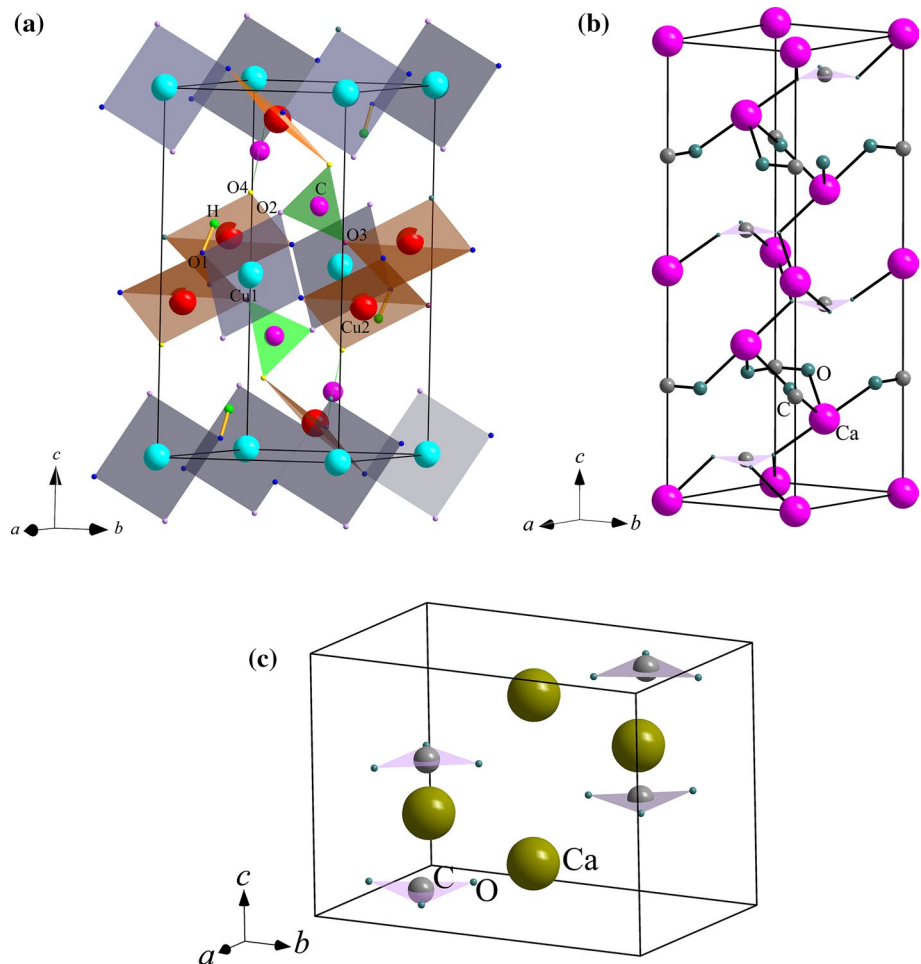


plate with a pre-indented thickness of about 50  $\mu\text{m}$  was used as the gasket, and a hole of 200  $\mu\text{m}$  in diameter was drilled to be used as the sample chamber. The sample along with a small piece of compressed gold powder with a methanol/ethanol/water mixture (16:3:1), which is a hydrostatic pressure-transmitting medium up to about 10 GPa (Angel et al. 2007), was loaded into the sample chamber. The equation of state of gold was employed to determine the experimental pressure (Fei et al. 2007). An image plate detector was used to collect the diffraction patterns, and the collecting time of each is 600 s, and 16 diffraction patterns were collected in this study. The diffraction patterns were integrated to generate the conventional one-dimensional profiles using the Fit2D program (Hammersley 1996). The unit cell parameters were calculated and refined with Le Bail method (Le Bail et al. 1988) through the software GSAS and the graphical interface EXPGUI (Larson and Von Dreele 2004).

Raman spectra were collected with Renishaw InVia spectrometer equipped with a Peltier-cooled charge-coupled device (CCD) detector. A 532-nm wavelength laser was used to excite the sample. The laser light was focused

using a Leica microscope with a long distance 20  $\times$  objective to a beam size of about 2  $\mu\text{m}$  diameter in the sample with the laser powder being 2 mW on the sample. No laser heating effects should occur under such conditions. A piece of single-crystal silicon was used to calibrate the wave numbers of the Raman shifts. For high-pressure measurements in a symmetric diamond anvil cell, a stainless steel foil (type T301) gasket was pre-indented to a thickness of  $\sim 55$   $\mu\text{m}$  and then drilled to a diameter of 200  $\mu\text{m}$ , served as the sample chamber. A ruby chip was loaded as pressure calibrant together with the azurite sample (80  $\times$  80  $\times$  30  $\mu\text{m}^3$ ) in the pre-indented T301 stainless steel gasket with a 200- $\mu\text{m}$  sample hole. Liquid argon was loaded as a pressure-transmitting medium using a liquid nitrogen cooling method. Ruby fluorescence spectra were collected before and after each collection of data, and the positions of the R1 and R2 peaks were determined by fitting with Lorentzian functions. Pressure was calculated from the fitted R1 and R2 peak positions using the method of Mao et al. (1986). All spectra were recorded in the backscattering geometry with no polarization used for the collected signal, and the collecting time was 160 s. The

manipulations of the obtained Raman spectra contained baseline adjustment and peak fitting.

## Results

The results of conventional X-ray diffraction at ambient conditions for azurite demonstrated that it is monoclinic with the refined lattice parameters  $a = 5.001$  (5) Å,  $b = 5.851$  (5) Å,  $c = 10.346$  (7) Å and  $\beta = 92.35$  (8)°. These values are in good agreement with  $a = 5.011$  (2) Å,  $b = 5.850$  (2) Å,  $c = 10.353$  (4) Å and  $\beta = 92.41$  (3)° reported by Belokoneva et al. (2001).

The room temperature and high-pressure X-ray diffraction data of azurite were recorded up to 11.08 GPa, and the typical diffraction patterns are shown in Fig. 2. All peaks shifted continuously toward higher  $2\theta$  angles with the exception of the almost fixed (002) peak. The variations of the d-spacings with pressure are continuous as shown in Fig. 3, and it displays that the (002) plane has inconspicuous shifts with increasing pressure as well. The diffraction patterns at high pressure show slightly peak-broadening, but neither sign of disappearance of peaks relative to the azurite structure nor the appearance of new peaks has been observed in the experimental process which indicates that the azurite is stable in present pressure range. The lattice parameters obtained by Le Bail profile fitting with GSAS (Fig. 4) at each pressure are listed in Table 1. The isothermal pressure–volume data were fitted with the third-order Birch–Murnaghan equation of state (III-BM-EoS) (Birch 1947):

$$P = (3/2)K_0 \left[ (V_0/V)^{7/3} - (V_0 - V)^{5/3} \right] \times \left\{ 1 + (3/4)(K'_0 - 4) \left[ (V_0 - V)^{2/3} - 1 \right] \right\}$$

where  $V_0$ ,  $V$ ,  $K_0$  and  $K'_0$  are the zero-pressure volume, high-pressure volume, isothermal bulk modulus and its pressure derivative, respectively. The least square fitting yielded  $V_0 = 304.5$  (4) Å<sup>3</sup>,  $K_0 = 40$  (2) GPa and  $K'_0 = 5.5$  (6). When fixing  $K'_0 = 4$ , the isothermal bulk modulus was determined as 45.1 (8) GPa. The unit cell volume data as a function of pressure and the compression curve calculated from these fitted parameters are shown in Fig. 5.

Each lattice parameter was fit to a linearized III-BM-EoS (Angel 2000) to obtain the linear EoS parameters, yielding:  $K_{a0} = 29.7$  (9) GPa,  $K_{b0} = 25.0$  (7) GPa and  $K_{c0} = 280$  (55) GPa for the  $a$ -,  $b$ - and  $c$ -axis, respectively. Figure 6 shows these parameters as functions of pressure. Then, we calculated the axial compressibilities (with  $\beta_d = 1/3K_0$ , where  $K_0$  is the isothermal bulk modulus at ambient conditions,  $\beta$  is the compressibility, and  $d$  is the unit cell parameter) of azurite and obtained  $\beta_a = 11.22 \times 10^{-3} \text{ GPa}^{-1}$ ,

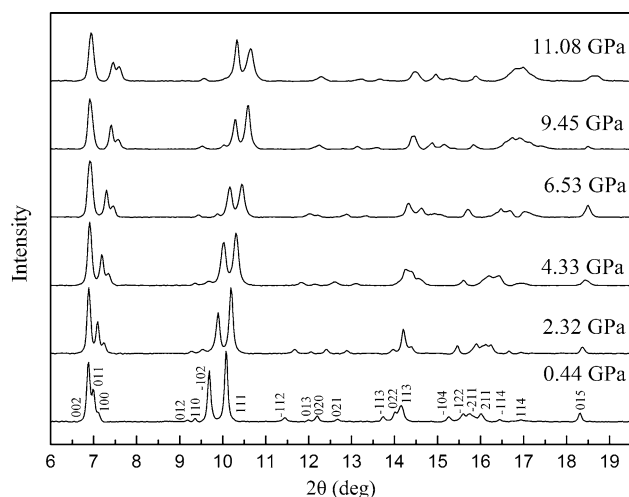


**Fig. 2** Representative X-ray diffraction patterns of azurite obtained in this study up to 11.08 GPa at room temperature

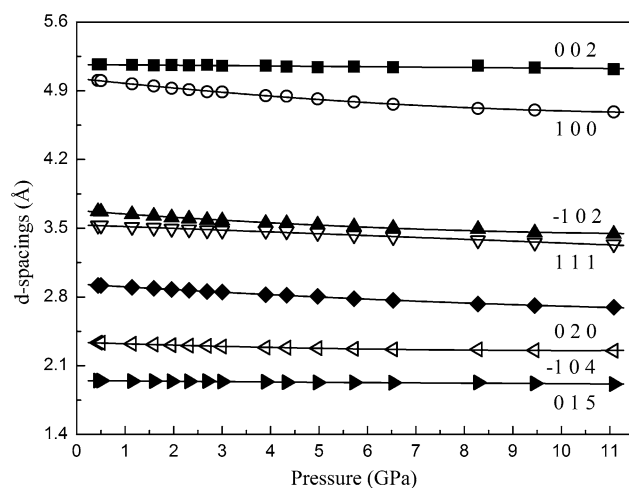


**Fig. 3** Evolution of the d-spacings of several crystallographic planes in azurite crystal structure with pressure

$\beta_b = 13.33 \times 10^{-3} \text{ GPa}^{-1}$  and  $\beta_c = 11.90 \times 10^{-2} \text{ GPa}^{-1}$  for  $a$ -,  $b$ - and  $c$ -axis, respectively. The elastic anisotropy of azurite can be expressed as:  $\beta_a:\beta_b:\beta_c = 9.43:11.20:1.00$ .

The volume Eulerian finite strain ( $f_E = [(V_0/V)^{2/3} - 1]/2$ ) versus ‘normalized pressure’ ( $F_E = P/[3f_E(2f_E + 1)^{5/2}]$ ) plot [ $f_E - F_E$  plot, (Angel 2000)] is shown in Fig. 7. The weighted linear fit of the data points yields the intercept value of  $F_E(0) = 39.6$  (7) GPa, which is consistent with the isothermal bulk modulus obtained by the III-BM-EoS ( $K_0 = 40$  (2) GPa). Furthermore, it is clear from Fig. 7 that the data points lie on an inclined straight line with a positive slope, which is consistent with a value of  $K'_0$  distinctly larger than 4 from III-BM-EoS (Angel 2000), showing that the  $P$ - $V$  data in this study can be well described by the III-BM-EoS.

At ambient conditions, fourteen bands in the range of 200–1200  $\text{cm}^{-1}$  were acquired from the Raman spectroscopy (Fig. 8). It is necessary to note that three bands were overlapped at about 400  $\text{cm}^{-1}$  and separated at high-pressure conditions. According to the results of previous studies (Frost et al. 2002; Mattei et al. 2008; Buzgar and Apopei 2009), the bands observed up to 600  $\text{cm}^{-1}$  (246.5, 264.7, 280.2, 330.1, 383.6, 398.9, 413.0 and 539.4  $\text{cm}^{-1}$ ) are assigned to the interactions between the Cu and O; the bands at 739.5 and 763.1  $\text{cm}^{-1}$  are attributed to the asymmetric  $[\text{CO}_3]^{2-}$  bending mode ( $\nu_4$ ); the bands assigned to

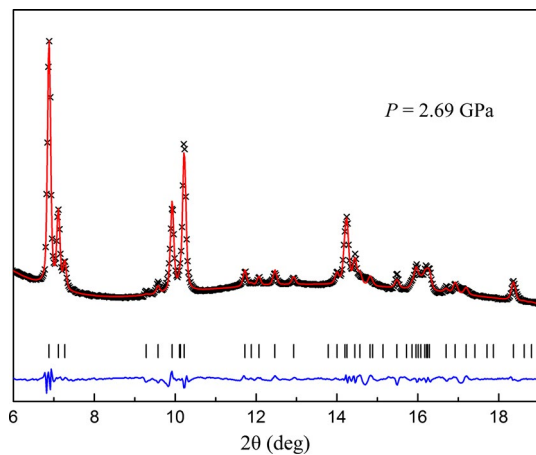


**Fig. 4** Le Bail profile fitting of the diffraction profiles at 2.69 GPa. Observed spectra (black line), fitted spectra (red solid line), difference plot (blue solid line) and Bragg peak positions (tick marks) are shown

the symmetric  $[\text{CO}_3]^{2-}$  bending mode ( $\nu_2$ ) appear at 813.3 and 834.3  $\text{cm}^{-1}$ ; the observed bands at 1093.4  $\text{cm}^{-1}$  are assigned to the symmetric  $[\text{CO}_3]^{2-}$  stretching mode ( $\nu_1$ ). The 939.9  $\text{cm}^{-1}$  mode is assigned to the O–H out-of-plane bending based on the results of previous Raman studies of azurite (Frost et al. 2002; Mattei et al. 2008; Buzgar and Apopei 2009). It is necessary to note that the O–H stretching mode at about 3400  $\text{cm}^{-1}$  (Frost et al. 2002; Mattei et al. 2008) and the O–H bending mode at about 1580  $\text{cm}^{-1}$  (Mattei et al. 2008; Buzgar and Apopei 2009) are out of the wave number range in this study.

The Raman spectra of azurite at selected pressures are also shown in Fig. 8, which shows the different evolutions of various vibrational groups with pressure. With increasing pressure, all the observed modes show a continuous shift to higher frequency. Figure 9 displays several Raman mode frequencies as a function of pressure. The  $[\text{CO}_3]^{2-}$  group exhibits a mode hardening and also exhibits a linear pressure dependence of frequency. The asymmetric  $[\text{CO}_3]^{2-}$  bending mode and the symmetric  $[\text{CO}_3]^{2-}$  stretching mode have positive linear slopes of 1.05 (5) and 1.27 (3)  $\text{cm}^{-1}/\text{GPa}$ , and the symmetric  $[\text{CO}_3]$  bending mode is almost fixed with a slope of 0.1 (1)  $\text{cm}^{-1}/\text{GPa}$ . Compared with the  $[\text{CO}_3]^{2-}$  group, the  $[\text{OH}]^-$  group is more sensitive to the pressures, and the O–H out-of-plane bending mode is characterized by a nonlinear response (Fig. 9). The variation of the O–H out-of-plane bending mode shows a nonlinear relation, but in the entire pressure range of this study, the sharp Raman bands assigned to vibrations of the azurite crystal structure are retained (Figs. 8, 9), indicating no evidence of any phase transition. Therefore, combining

**Table 1** Lattice parameters and volume versus pressure for azurite at room temperature

$P$ (GPa)	$a$ (Å)	$b$ (Å)	$c$ (Å)	$\beta$ (°)	$V$ (Å <sup>3</sup> )
0.44 (2)	5.0025 (3)	5.8312 (5)	10.3293 (4)	92.401 (4)	301.05 (3)
0.50 (3)	4.9992 (3)	5.8276 (6)	10.3275 (4)	92.316 (5)	300.63 (4)
1.14 (6)	4.9648 (4)	5.7918 (5)	10.3155 (4)	91.982 (5)	296.45 (4)
1.59 (8)	4.9436 (3)	5.7734 (4)	10.3058 (4)	91.763 (5)	294.00 (3)
1.96 (10)	4.9189 (3)	5.7469 (4)	10.3077 (4)	91.467 (5)	291.29 (3)
2.32 (12)	4.9043 (3)	5.7306 (4)	10.3054 (5)	91.318 (4)	289.55 (3)
2.69 (13)	4.8894 (4)	5.7104 (4)	10.3304 (4)	91.064 (6)	288.33 (3)
3.00 (15)	4.8797 (3)	5.6977 (5)	10.2941 (4)	91.045 (5)	286.16 (4)
3.90 (20)	4.8414 (4)	5.6420 (5)	10.2975 (5)	90.696 (5)	281.26 (4)
4.33 (22)	4.8322 (7)	5.6242 (8)	10.2754 (7)	90.827 (9)	279.23 (6)
4.97 (23)	4.8105 (5)	5.6063 (6)	10.2618 (6)	90.724 (9)	276.73 (4)
5.72 (30)	4.7789 (5)	5.5619 (6)	10.2720 (5)	90.451 (7)	273.02 (4)
6.53 (33)	4.7561 (7)	5.5254 (7)	10.2625 (7)	90.351 (13)	269.69 (6)
8.28 (41)	4.7138 (6)	5.4519 (9)	10.2957 (5)	89.660 (12)	264.57 (6)
9.45 (47)	4.6957 (5)	5.4211 (7)	10.2516 (7)	89.635 (10)	260.96 (5)
11.08 (58)	4.6778 (7)	5.3879 (9)	10.2201 (9)	89.564 (14)	257.58 (6)

Numbers in parenthesis represent the relative error calculated for lattice parameters, volume and pressure

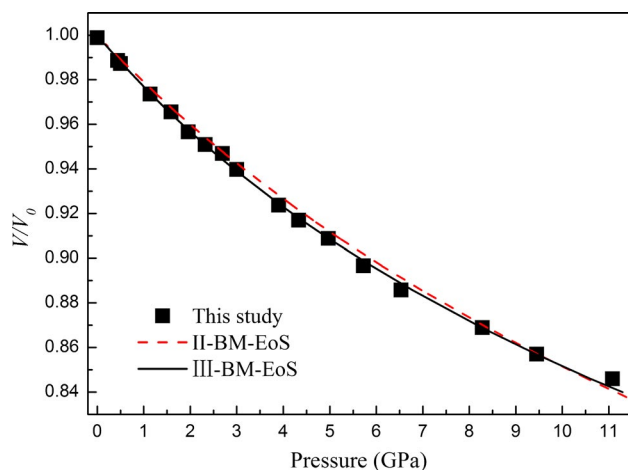


**Fig. 5**  $P$ - $V$  data of azurite at room temperature. A third-order Birch–Murnaghan equation of state fitted with  $K_0$  and  $K'_0$  is 40 GPa and 5.5, respectively. In addition, the second-order Birch–Murnaghan equation of state fit is also shown for comparison. The *error bars* of the data points are smaller than the *symbols*

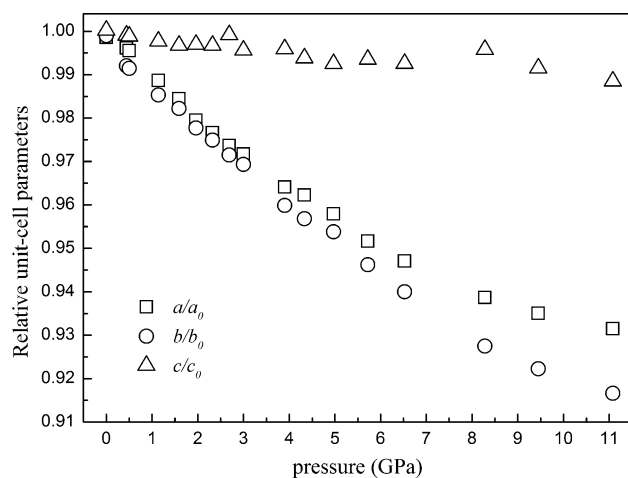


**Fig. 6** Pressure dependence of the unit cell parameters  $a$ ,  $b$ , and  $c$  of azurite at room temperature. Note that the *error bars* of the data points are smaller than the *symbols*

the results of high-pressure X-ray study (Figs. 2, 3), there should be no phase transitions on azurite within the pressure range in this study.

## Discussion

Merlini et al. (2012) investigated the high-pressure behavior of another basic hydrous copper carbonate mineral, malachite  $[\text{Cu}_2(\text{OH})_2\text{CO}_3]$ , and concluded that it undergoes a phase transition from malachite structure to rosasite structure at 6 GPa. The pressure–volume data of malachite were

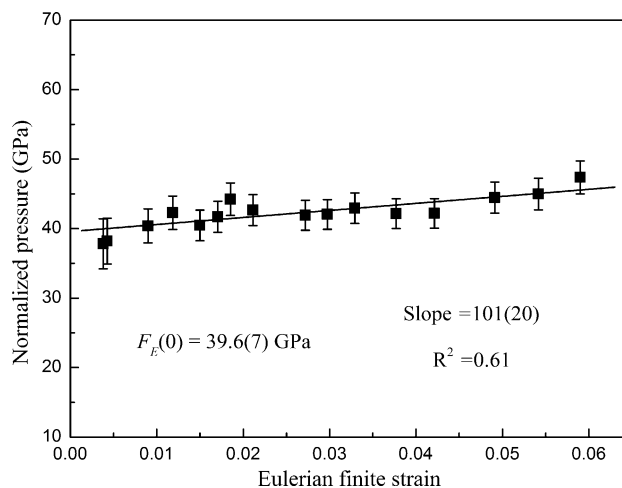


**Fig. 7** Volume Eulerian strain–normalized pressure ( $F_E - f_E$ ) plot. The *solid line* is the linear fit of the data

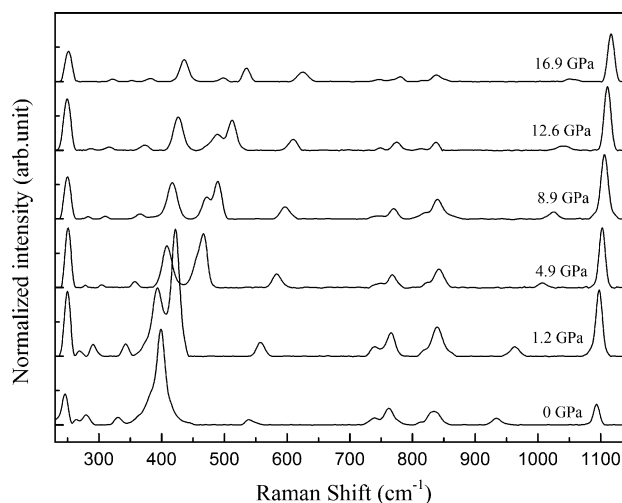


**Fig. 8** Representative Raman spectra of azurite up to 16.9 GPa

fitted with the III-BM-EoS, and the isothermal bulk modulus was obtained as  $K_0 = 43$  (3) GPa [ $K'_0 = 9.2$  (16)]. But in this study of azurite, there are no signs of phase transitions from data of high-pressure X-ray diffraction and Raman spectra. Malachite is also monoclinic (space group  $P2_1/a$ ), but the copper ions in this structure are six coordinated to oxygen ions which is quite different to azurite (monoclinic with space group  $P2_1/c$ ) that has copper ions with four coordinated to oxygen ions. This may be an explanation why azurite has no phase transition within the same pressure region. In this study, the isothermal bulk modulus of azurite was obtained as  $K_0 = 40$  (2) GPa which is very consistent with that of malachite ( $K_0 = 43$  (3) GPa) within their uncertainties, indicating that the difference in structure has very limited effect on their values of bulk modulus.

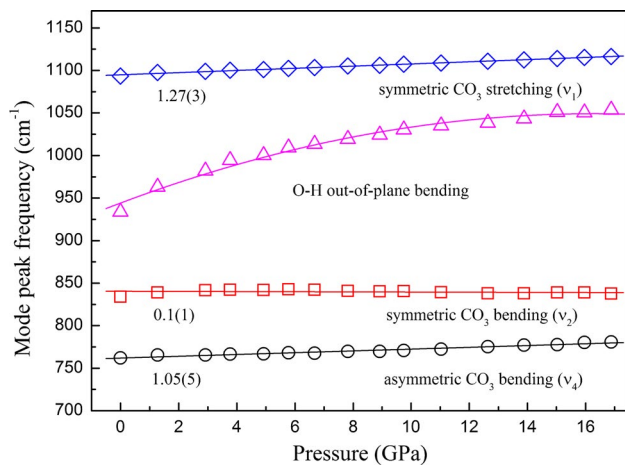


**Fig. 9** Pressure dependences of the observed Raman modes for azurite up to 16.9 GPa

Zhang and Reeder (1999) systematically investigated the comparative compressibilities of calcite group carbonates and showed that the bulk modulus has an approximately inverse linear correlation with ambient cell volume (or the radius of metal cation). They also found that magnesite [MgCO<sub>3</sub>] and calcite [CaCO<sub>3</sub>], as the most abundant carbonates in the Earth, are clearly incongruent with the bulk modulus–cell volume linear trend, which is defined by the behavior of other calcite group minerals (gaspeite [NiCO<sub>3</sub>], rhodochrosite [MnCO<sub>3</sub>], siderite [FeCO<sub>3</sub>], smithsonite [ZnCO<sub>3</sub>], spherocobaltite [CoCO<sub>3</sub>] and otavite [CdCO<sub>3</sub>]). The different outer electron configurations of metal cations can be an explanation (Zhang and Reeder 1999). The aragonite and dolomite group carbonates also gain sufficient attentions on their compressibilities, but no systematic comparative studies like calcite group have been carried on (e.g., Martinez et al. 1996; Ono et al. 2005; Zhang et al. 2013; Holl et al. 2000; Ross and Reeder 1992). The bulk modulus ( $K_0$ ) and effective ionic radii of metal cations ( $M^{2+}$ ) of three types anhydrous carbonates, hydrous carbonate malachite and azurite are summarized in Table 2. Table 2 shows that the bulk modulus of aragonite and dolomite group carbonates also has negative correlations with the size of the metal cations. Except that calcite and aragonite have approximate values of bulk modulus, the aragonite group ( $K_0 = 50\text{--}63$  GPa) has larger compressibilities compared with calcite group ( $K_0 = 89\text{--}131$  GPa), which can be explained by their larger metal cations. According to Table 2, in general, the bulk modulus or compressibilities of anhydrous carbonates can be largely controlled by the size of metal cations, that is, the minerals with large cations should be more compressible (Anderson and Anderson 1970). Nevertheless, other factors like electronic structure of divalent cations can partly affect the compressibilities (Zhang and Reeder 1999).

The  $K_0$  values (50–131 GPa) of anhydrous carbonates are obviously larger than that of malachite (43 GPa) from Merlini et al. (2012) and azurite (40 GPa) in this study (Table 2). The bulk modulus describes a substance's resistance to uniform compression (Halliday et al. 2010), so the smaller values of  $K_0$  indicate that the mineral malachite and azurite are much more compressible compared with anhydrous carbonate minerals. The effective ionic radius of metal cations (Cu) in malachite and azurite is relatively smaller compared to that of anhydrous carbonates (Table 2), but on the contrary, they do not have relatively large values of  $K_0$ . The values of  $K_0$  of calcite (67–73 GPa) and aragonite (64–73 GPa) are similar; likewise, malachite (43 GPa) and azurite (40 GPa) also have approximate values of  $K_0$ . Thus, the structural difference has little effect on the bulk modulus of calcite and aragonite as well as malachite and azurite. We infer that azurite and malachite have distinctly larger compressibilities than that of calcite group, aragonite group and dolomite group carbonates, which can be largely attributed to the [OH]<sup>−</sup> group in structures. The [OH]<sup>−</sup> group has dramatic effects on the compressibilities of minerals according to the previous studies (e.g., Smyth et al. 2005; Lager et al. 2002; Jacobsen 2006; Fan et al. 2013; Xu et al. 2014). The isothermal bulk modulus of hydrous olivine (Mg<sub>1.84</sub>Fe<sub>0.09</sub>SiH<sub>0.127</sub>O<sub>4</sub>, water content 0.8 wt %) was measured as 120 (2) GPa (Smyth et al. 2005), which is 7 % smaller than that of the anhydrous olivine [(Mg<sub>0.9</sub>Fe<sub>0.1</sub>)<sub>2</sub>SiO<sub>4</sub>] ( $K_0 = 129$  (6) GPa) (Zha et al. 1998). In addition, the hydrous grossular [Ca<sub>3</sub>Al<sub>2</sub>(H<sub>4</sub>O<sub>4</sub>)<sub>3</sub>] containing water content 29 wt% has a much smaller isothermal bulk modulus (58 (1) GPa) (Lager et al. 2002) compared to the anhydrous grossular [Ca<sub>3</sub>Al<sub>2</sub>Si<sub>3</sub>O<sub>12</sub>] ( $K_0 = 169.3$  (12) GPa) (Pavese et al. 2001). Therefore, we infer that the [OH]<sup>−</sup> group in malachite and azurite structures can result in much smaller isothermal bulk modulus relative to the anhydrous carbonates.

The largely intense compression anisotropy of azurite, which is expressed by  $\beta_a:\beta_b:\beta_c = 9.43:11.20:1.00$ , can be the most striking property of azurite at high pressure. It demonstrates that the *a*- and *b*-axis are close to ten times more compressible than the *c*-axis as shown in Fig. 6. Figures 2 and 3 also show that the *d*-spacing of the lattice plane (002), which is parallel to the *ab*-plane, is not sensitive to the increasing pressure. The similar anisotropy also exists in the structure of malachite, and the only difference is that the *b*-axis is the most rigid (Merlini et al. 2012). The compressibilities of anhydrous carbonates also present distinctive anisotropy based on the previous studies. The anisotropic nature of the compression is a common feature for all carbonate minerals. For most calcite group carbonates, the *c*-axis is about 2–3 times more compressible than the *ab*-plane (Gao et al. 2014b; Zhang and Reeder 1999; Redfern and Angel 1999; Fiquet and Reynard

**Table 2** Comparison of elastic parameters of carbonate minerals

	$K_0$ (GPa)	$K''_0$	$r_M^{2+}$ (Å)	References
<i>Calcite group</i>				
Calcite (CaCO <sub>3</sub> )	73.46 (27)	4 (fixed)	1.00	Redfern and Angel (1999)
	67 (2)	4 (fixed)		Zhang and Reeder (1999)
Gaspeite (NiCO <sub>3</sub> )	131 (1)	4 (fixed)	0.69	Zhang and Reeder (1999)
Otavite (CdCO <sub>3</sub> )	97 (1)	4 (fixed)	0.95	Zhang and Reeder (1999)
	89.1 (9)	3.39 (5)		Minch et al. (2010b)
	101 (3)	2.1 (3)		
Magnesite (MgCO <sub>3</sub> )	117 (3)	2.3 (7)	0.72	Ross (1997)
	111 (1)	4 (fixed)		
	114 (1)	4 (fixed)		Fiquet and Reynard (1999)
	92 (8)	9.1 (2.2)		
Rhodochrosite (MnCO <sub>3</sub> )	108 (1)	4 (fixed)	0.83	Zhang and Reeder (1999)
	126 (10)	4 (fixed)		Ono (2007a)
Siderite (FeCO <sub>3</sub> )	117.1 (8)	4 (fixed)	0.78	Lavina et al. (2010)
	110 (2)	4.6 (2)		
	120 (3)	4.3 (3)		Nagai et al. (2010)
Smithsonite (ZnCO <sub>3</sub> )	124 (1)	4 (fixed)	0.74	Zhang and Reeder (1999)
	126.8 (6)	4 (fixed)		Gao et al. (2014b)
Spherochalcite (CoCO <sub>3</sub> )	125 (1)	4 (fixed)	0.745	Zhang and Reeder (1999)
<i>Aragonite group</i>				
Aragonite (CaCO <sub>3</sub> )	64.8	4 (fixed)	1.00	Martinez et al. (1996)
	65.4	2.7		
	67.1 (6.3)	4.7 (0.8)		Ono et al. (2005)
	73.1 (2.2)	4 (fixed)		
Cerussite (PbCO <sub>3</sub> )	63 (3)	4 (fixed)	1.19	Zhang et al. (2013)
Witherite (BaCO <sub>3</sub> )	50.4 (12)	1.9 (4)	1.35	Holl et al. (2000)
<i>Dolomite group</i>				
Dolomite (CaMg(CO <sub>3</sub> ) <sub>2</sub> )	94.1 (7)	4 (fixed)	1.00, 0.72	Ross and Reeder (1992)
	94.1 (4)	4 (fixed)		Mao et al. (2011)
Ankerite (CaFe(CO <sub>3</sub> ) <sub>2</sub> )	91.7 (4)	4 (fixed)	1.00, 0.78	Ross and Reeder (1992)
Norsethite (BaMg(CO <sub>3</sub> ) <sub>2</sub> )	64.6 (7)	4 (fixed)	1.35, 0.72	Pippinger et al. (2014)
	66.2 ± 2.3	2.0 ± 1.8		
<i>Carbonates with hydroxide</i>				
Azurite (Cu <sub>3</sub> (CO <sub>3</sub> ) <sub>2</sub> (OH) <sub>2</sub> )	40 (2)	5.5 (6)	0.57	This study
	45.1 (8)	4 (fixed)		
Malachite (Cu <sub>2</sub> CO <sub>3</sub> (OH) <sub>2</sub> )	43 (3)	9.2 (16)	0.73	Merlini et al. (2012)

$r_M^{2+}$  effective ionic radii of metal cations from Shannon (1976)

1999), while the *c*-axis is about six times more compressible in CdCO<sub>3</sub> structure (Minch et al. 2010b; Zhang and Reeder 1999). In addition, witherite [BaCO<sub>3</sub>] has the most intense compression anisotropy among the aragonite group, and the *c*-axis is about 10 times more compressible than the *a*- and *b*-axis (Holl et al. 2000). Aragonite [CaCO<sub>3</sub>] and cerussite [PbCO<sub>3</sub>] have similar compression anisotropies, which shows that the *c*-axis is the most compressible, the *a*-axis is the most rigid, and the *b*-axis has a mean linear compressibility (Zhang et al. 2013; Martinez et al. 1996). Furthermore, dolomite group carbonates

display approximate behavior of compression anisotropies to that of calcite group, and the *c*-axis is approximately three times more compressible than the *a*-axis in both dolomite [CaMg(CO<sub>3</sub>)<sub>2</sub>] and ankerite [CaFe(CO<sub>3</sub>)<sub>2</sub>] structure (Martinez et al. 1996; Ross and Reeder 1992). The rigid [CO<sub>3</sub>]<sup>2-</sup> groups and the more compressible [MO<sub>6</sub>] octahedra are two basic building blocks in anhydrous carbonates structure (Redfern 2000) that control the behaviors of compression anisotropy. Thus, the directions parallel to the planar [CO<sub>3</sub>]<sup>2-</sup> groups have larger incompressibilities, and directions which are perpendicular to the [CO<sub>3</sub>]<sup>2-</sup> groups

**Table 3** Pressure shifts of the Raman modes [ $dv/dP$  ( $\text{cm}^{-1}/\text{GPa}$ )] of  $[\text{CO}_3]^{2-}$  group in certain carbonates

	$\nu_1$	$\nu_2$	$\nu_3$	$\nu_4$	References
Calcite ( $\text{CaCO}_3$ )	5.9 (4)		9.0 (5)	2.2 (2)	Gillet et al. (1993)
Otavite ( $\text{CdCO}_3$ )	3.12 (9)		1.44 (4)	1.44 (4)	Minch et al. (2010b)
Magnesite ( $\text{MgCO}_3$ )	2.5 (3)		4.0 (4)	1.4 (2)	Gillet et al. (1993)
Magnesian siderite ( $\text{Mg}_{0.35}\text{Fe}_{0.65}\text{CO}_3$ )	2.17 (7)			1.49 (6)	Lin et al. (2012)
Rhodochrosite ( $\text{MnCO}_3$ )	1.906			0.946	Farfan et al. (2013)
Siderite ( $\text{FeCO}_3$ )	2.20				Farfan et al. (2012)
Aragonite ( $\text{CaCO}_3$ )	2.7 (3)			1.6 (3)	Gillet et al. (1993)
Witherite ( $\text{BaCO}_3$ )	3.2			2.0	Lin and Liu (1997a, b)
Dolomite ( $\text{CaMg}(\text{CO}_3)_2$ )	2.9 (3)		3.5 (3)	1.6 (3)	Gillet et al. (1993)
Azurite ( $\text{Cu}_3(\text{CO}_3)_2(\text{OH})_2$ )	1.27 (3)	0.1 (1)		1.05 (5)	This study

$\nu_1$  symmetric stretching mode;  $\nu_2$  symmetric bending mode;  $\nu_3$  asymmetric stretching mode;  $\nu_4$  symmetric bending mode

are more compressible. As a result, the  $c$ -axis has much smaller incompressibility than that of the  $a$ - and  $b$ -axis in calcite group, aragonite group and dolomite group carbonates (Fig. 1b, c). Likewise, the anisotropy of azurite can be explained on the basis of the structure. The  $[\text{CO}_3]^{2-}$  groups in azurite structure are almost parallel to the  $c$ -axis (Fig. 1a), and thus, the  $c$ -axis is much less compressible than the  $a$ - and  $b$ -axis. Possibly for the same reason, malachite shows the similar compression anisotropy to azurite. The compression anisotropy of azurite is distinctly more intense than that of the most anhydrous carbonates, which may mainly due to that the  $[\text{OH}]^-$  groups in the azurite structure greatly increase the compressibilities of the  $a$ - and the  $b$ -axis. Other possible reasons are discussed below.

Anhydrous carbonates have two types of Raman modes, that is, the internal modes ( $[\text{CO}_3]^{2-}$  group) and the lattice modes. In comparison, hydrous carbonates not only have these two types but one type of the vibrations of  $[\text{OH}]^-$  group. In this study of Raman spectroscopy on azurite, we can obtain that the pressure has great influence on the vibration of the  $[\text{OH}]^-$  group (Figs. 8, 9), which dramatically illustrates that the  $[\text{OH}]^-$  is a weak group in azurite structure, and this high-pressure characteristic of  $[\text{OH}]^-$  also evidences the large effect of hydroxyl on the smaller isothermal bulk modulus of azurite and malachite. On the contrary, the high-pressure Raman spectroscopy indicates the large incompressibility of the  $[\text{CO}_3]^{2-}$  groups, which support the explanation of the compressional anisotropy of azurite from the in situ X-ray diffraction experiment in this study. In the Raman modes of  $[\text{CO}_3]^{2-}$  groups, the vibrations of  $\nu_1$  and  $\nu_4$  are both in plane, but  $\nu_2$  is out of plane (Frost et al. 2002).  $\nu_1$  and  $\nu_4$  show a linear shift with pressure appropriately, while  $\nu_2$  is not well with a linear description (Fig. 9). Likewise, the O–H out-of-plane bending mode at  $933.9 \text{ cm}^{-1}$  shows a nonlinear shift with pressure (Fig. 9), which is so different to the response of

$\nu_1$  and  $\nu_4$ . Possibly, the nonlinear response of the O–H bending mode and  $\nu_2$  mode to pressure may be caused by their out-of-plane vibration modes. Table 3 summarizes the high-pressure Raman spectroscopy results of the  $[\text{CO}_3]^{2-}$  groups in certain anhydrous carbonates and azurite in this study, which shows that the values of  $dv/dP$  of  $\nu_1$  ( $1.27 (3) \text{ cm}^{-1}/\text{GPa}$ ) and  $\nu_4$  ( $1.05 (5) \text{ cm}^{-1}/\text{GPa}$ ) modes in azurite are clearly smaller than that of other anhydrous carbonates ( $dv/dP(\nu_1) = 1.9\text{--}5.9 \text{ cm}^{-1}/\text{GPa}$  and  $dv/dP(\nu_4) = 1.4\text{--}2.2 \text{ cm}^{-1}/\text{GPa}$ ) with the exception of the smaller  $\nu_4$  ( $dv/dP = 0.946 \text{ cm}^{-1}/\text{GPa}$ ) in rhodochrosite ( $\text{MnCO}_3$ ). This may indicate that the  $[\text{CO}_3]^{2-}$  groups in azurite are less sensitive to the increasing pressure than that of most anhydrous carbonates, namely the  $[\text{CO}_3]^{2-}$  groups in azurite are more rigid. Thus, this could be another reason of the distinct more intense compression anisotropy in azurite structure than that of most anhydrous carbonates. On the whole, the results of high-pressure X-ray diffraction and Raman spectroscopy studies show the consistency on the smaller isothermal bulk modulus and elastic anisotropy of azurite.

In calcite group, calcite [ $\text{CaCO}_3$ ] transforms into aragonite at a relatively low pressure ( $\sim 2 \text{ GPa}$ ) and high temperature (Suito et al. 2001), the aragonite to post-aragonite structure ( $Pm\bar{m}n$ ) transition occurs at  $\sim 40 \text{ GPa}$  (Ono et al. 2007), and the pyroxene-type structure with space group  $C222_1$  obtained above  $\sim 137 \text{ GPa}$  (Oganov et al. 2006, 2008; Ono et al. 2007). In addition, a calcite-type to an aragonite-type structure phase transition of otavite [ $\text{CdCO}_3$ ] at  $18\text{--}25 \text{ GPa}$  and  $\sim 1000 \text{ }^\circ\text{C}$  was reported by Liu and Lin (1997), and afterward Minch et al. (2010b) also observed a phase transition of otavite at  $\sim 19 \text{ GPa}$ , but the structure of the new phase was not aragonite type. Rhodochrosite [ $\text{MnCO}_3$ ] transforms to a new orthorhombic structure at  $\sim 50 \text{ GPa}$ ; however, the new phase is different from aragonite type (Ono 2007a). Furthermore, the path of phase transition of magnesite [ $\text{MgCO}_3$ ] is markedly different

from calcite; magnesite [MgCO<sub>3</sub>] is stable at high-pressure and high-temperature condition of the Earth's lower mantle (Isshiki et al. 2004; Oganov et al. 2008) and then occurs a pyroxene structure at 113 GPa and a CaTiO<sub>3</sub> calcite structure at 200 GPa (Isshiki et al. 2004; Skorodumova et al. 2005). Last, siderite [FeCO<sub>3</sub>] experiences an isostructural transformation of electronic transition at 46–50 GPa (Lavina et al. 2009; Farfan et al. 2012). The paths of phase transitions of calcite group carbonates above show that the phase transition pressure of calcite (~2 GPa) is the lowest, and magnesite has the highest phase transition pressure (~113 GPa). Their phase transition pressures may be partly controlled by the size of the metal cations in structure (Gao et al. 2014b), and the Mg<sup>2+</sup> ion has the smallest size (Table 2), so its phase transition pressure is the largest. Similarly, the types of phase transitions are also diverse for the aragonite group carbonates. In aragonite group, witherite [BaCO<sub>3</sub>] transforms to post-aragonite structure on heating at 9–10 GPa (Ono 2007b; Townsend et al. 2013) and then remains stable up to 150 GPa and 2000 K (Townsend et al. 2013), whereas cerussite [PbCO<sub>3</sub>] and strontianite [SrCO<sub>3</sub>] both undergo the aragonite to post-aragonite transition at 17 and 35 GPa, respectively (Lin and Liu 1997a, b). From the above discussions about the anhydrous carbonates, we can find that for isostructural carbonates, their phase transition conditions are not necessarily the same. Likewise, for the hydrous carbonates, the phase transition conditions between malachite and azurite are also not the same, in which malachite [Cu<sub>2</sub>(OH)<sub>2</sub>CO<sub>3</sub>] undergoes a phase transition from malachite structure to rosasite structure at ~6 GPa (Merlini et al. 2012), but azurite [Cu<sub>3</sub>(CO<sub>3</sub>)<sub>2</sub>(OH)<sub>2</sub>] is stable up to ~16 GPa in this study. However, further investigation at higher pressures and temperatures will be needed to confirm the structural stability of azurite.

On the basis of the results of the high-pressure X-ray diffraction and Raman spectroscopy of azurite in this study, the [OH]<sup>−</sup> group in its structure has a great influence on its compressibility. Accordingly, it can be inferred that hydroxyl in the structures of anhydrous carbonates can strongly affect their physical properties. First, the incorporation of hydrogen in the structure of anhydrous can largely reduce the isothermal bulk modulus. Additionally, the compressional anisotropies of these carbonates can be possibly affected. Last, the structural stabilities may also be modified, because the hydroxyl can affect the phase boundaries (Ohtani 2006). Hence, the presence of hydroxyl in the structure of carbonates can largely affect our knowledge of the composition of the Earth's interior, and it is necessary to take into account the effect of hydroxyl of on carbonates when modeling the Earth's global carbon cycle and investigating the influence of carbonates on the physical and chemical properties of the Earth's mantle.

## Conclusion

The high-pressure in situ angle-dispersive X-ray diffraction and Raman spectroscopy combined with diamond anvil cells were employed to investigate the high-pressure behavior of natural azurite [Cu<sub>3</sub>(CO<sub>3</sub>)<sub>2</sub>(OH)<sub>2</sub>] up to 11 and 16 GPa at room temperature, respectively. The results of Raman spectroscopy and X-ray diffraction experiments show that no phase transitions occur within the pressure range. The isothermal pressure–volume data can be well described by the third-order Birch–Murnaghan EoS with  $V_0 = 304.5$  (4) Å<sup>3</sup>,  $K_0 = 40$  (2) GPa and  $K'_0 = 5.5$  (6). The lower  $K_0$  value in comparison with anhydrous carbonates can be largely attributed to the [OH]<sup>−</sup> groups in azurite structure. Axial compressibilities show considerable anisotropy with  $K_{a0} = 29.7$  (9) GPa,  $K_{b0} = 25.0$  (7) GPa and  $K_{c0} = 280$  (55) GPa, and the rigid [CO<sub>3</sub>]<sup>2−</sup> groups in azurite which are almost parallel to the *c*-axis should be an explanation. In addition, we infer that the stabilities and compressional anisotropies of typical anhydrous carbonates may be greatly affected by hydroxyl in their structures.

**Acknowledgments** We thank Prof. Guohong Gong for his help with the conventional powder X-ray analysis and the beamline scientists of BL15U1 of the Shanghai Synchrotron Radiation Facility (SSRF) and 4W2 of the Beijing Synchrotron Radiation Facility (BSRF) for the technical help. This work is supported by the National Natural Science Foundation of China (Grant Nos. 41374107 and 41274105), the Youth Innovative Technology Talents program of Institute of geochemistry, Chinese academy of Sciences (2013, to Dawei Fan) and the Western Doctor Special fund of the West Light Foundation of Chinese academy of Sciences (2011, to Dawei Fan).

## References

- Anderson DL, Anderson OL (1970) The bulk modulus–volume relationship for oxides. *J Geophys Res* 75:3494–3500
- Angel RJ (2000) Equations of state. *Rev Mineral Geochem* 41:35–59
- Angel RJ, Bujak M, Zhao J, Gatta GD, Jacobsen SD (2007) Effective hydrostatic limits of pressure media for high-pressure crystallographic studies. *J Appl Crystallogr* 40:26–32
- Anthony JW, Bideaux RA, Bladh KW, Nichols MC (1995) *Handbook of mineralogy*. Mineral Data Publ, Tucson
- Belokoneva E, Gubina YK, Forsyth J (2001) The charge density distribution and antiferromagnetic properties of azurite Cu<sub>3</sub>[CO<sub>3</sub>]<sub>2</sub>(OH)<sub>2</sub>. *Phys Chem Miner* 28:498–507
- Birch F (1947) Finite elastic strain of cubic crystals. *Phys Rev* 71:809–824
- Boulard E, Menguy N, Auzende A, Benzerara K, Bureau H, Antonangeli D, Corgne A, Morard G, Siebert J, Perrillat JP (2012) Experimental investigation of the stability of Fe-rich carbonates in the lower mantle. *J Geophys Res* 117:B02208
- Brenker FE, Vollmer C, Vincze L, Vekemans B, Szymanski A, Janssens K, Szaloki I, Nasdala L, Joswig W, Kaminsky F (2007) Carbonates from the lower part of transition zone or even the lower mantle. *Earth Planet Sci Lett* 260:1–9
- Buob A, Luth RW, Schmidt MW, Ulmer P (2006) Experiments on CaCO<sub>3</sub>-MgCO<sub>3</sub> solid solutions at high pressure and temperature. *Am Miner* 91:435–440

- Buzgar N, Apopei AI (2009) The Raman study of certain carbonates. *Geologie Tomul L* 2:97–112
- Chaney J, Santillán JD, Knittle E, Williams Q (2014) A high-pressure infrared and Raman spectroscopic study of BaCO<sub>3</sub>: the aragonite, trigonal and *Pmmn* structures. *Phys Chem Miner*. doi:10.1007/s00269-014-0702-0
- Dasgupta R, Hirschmann MM (2010) The deep carbon cycle and melting in Earth's interior. *Earth Planet Sci Lett* 298:1–13
- Dasgupta R, Chi H, Shimizu N, Buono AS, Walker D (2013) Carbon solution and partitioning between metallic and silicate melts in a shallow magma ocean: implications for the origin and distribution of terrestrial carbon. *Geochim Cosmochim Acta* 102:191–212
- Fan DW, Wei SY, Xie HS (2013) An in situ high-pressure X-ray diffraction experiment on hydroxyapophyllite. *Chin Phys B* 22:010702
- Farfan G, Wang SB, Ma HW, Caracas R, Mao WL (2012) Bonding and structural changes in siderite at high pressure. *Am Miner* 97:1421–1426
- Farfan GA, Boulard E, Wang S, Mao WL (2013) Bonding and electronic changes in rhodochrosite at high pressure. *Am Mineral* 98:1817–1823
- Fei YW, Ricolleau A, Frank M, Mibe K, Shen G, Prakapenka V (2007) Toward an internally consistent pressure scale. *Proc Natl Acad Sci USA* 104:9182–9186
- Fiquet G, Reynard B (1999) High-pressure equation of state of magnesite: new data and a reappraisal. *Am Mineral* 84:856–860
- Frost RL, Martens WN, Rintoul L, Mahmutagic E, Klopogge JT (2002) Raman spectroscopic study of azurite and malachite at 298 and 77 K. *J Raman Spectrosc* 33:252–259
- Gaillard F, Malki M, Iacono-Marziano G, Pichavant M, Scaillet B (2008) Carbonate melts and electrical conductivity in the asthenosphere. *Science* 322:1363–1365
- Gao J, Huang WF, Wu X, Fan DW, Wu ZY, Xia DG, Qin S (2014a) Compressibility of carbonophosphate bradleyite Na<sub>3</sub>Mg(CO<sub>3</sub>)(PO<sub>4</sub>) by X-ray diffraction and Raman spectroscopy. *Phys Chem Miner*. doi:10.1007/s00269-014-0710-0
- Gao J, Zhu F, Lai XJ, Huang R, Qin S, Chen DL, Liu J, Zheng LR, Wu X (2014b) Compressibility of a natural smithsonite ZnCO<sub>3</sub> up to 50 GPa. *High Press Res* 34:89–99
- Gattow Gv, Zemann J (1958) Neubestimmung der Kristallstruktur von Azurite, Cu<sub>3</sub>(OH)<sub>2</sub>(CO<sub>3</sub>)<sub>2</sub>. *Acta Crystallogr* 11:866–872
- Gillet P, Biellmann C, Reynard B, McMillan P (1993) Raman spectroscopic studies of carbonates Part I: high-pressure and high-temperature behaviour of calcite, magnesite, dolomite and aragonite. *Phys Chem Miner* 20:1–18
- Halliday D, Resnick R, Walker J (2010) *Fundamentals of physics extended*. Wiley, New York
- Hammersley J (1996) Fit2D report. European Synchrotron Radiation Facility, Grenoble
- Holl C, Smyth J, Laustsen H, Jacobsen S, Downs R (2000) Compression of witherite to 8 GPa and the crystal structure of BaCO<sub>3</sub>II. *Phys Chem Miner* 27:467–473
- Isshiki M, Irifune T, Hirose K, Ono S, Ohishi Y, Watanuki T, Nishibori E, Takata M, Sakata M (2004) Stability of magnesite and its high-pressure form in the lowermost mantle. *Nature* 427:60–63
- Jacobsen SD (2006) Effect of water on the equation of state of nominally anhydrous minerals. *Rev Mineral Geochem* 62:321–342
- Jana D, Walker D (1997) The impact of carbon on element distribution during core formation. *Geochim Cosmochim Acta* 61:2759–2763
- Kepler H, Wiedenbeck M, Shcheka SS (2003) Carbon solubility in olivine and the mode of carbon storage in the Earth's mantle. *Nature* 424:414–416
- Klein C, Hurlbut CS, Dana JD (1993) *Manual of mineralogy*. Wiley, New York
- Lager GA, Downs RT, Origlieri M, Garoutte R (2002) High-pressure single-crystal X-ray diffraction study of katoite hydrogarnet: evidence for a phase transition from *Ia3d* → *Ir<sub>M</sub><sup>2+</sup>* symmetry at 5 GPa. *Am Mineral* 87:642–647
- Larson AC, Von Dreele RB (2004) General structure analysis system (GSAS). Los Alamos National Laboratory Report LAUR 86-748
- Lavina B, Dera P, Downs RT, Prakapenka V, Rivers M, Sutton S, Nicol M (2009) Siderite at lower mantle conditions and the effects of the pressure-induced spin-pairing transition. *Geophys Res Lett* 36:L23306
- Lavina B, Dera P, Downs RT, Yang W, Sinogeikin S, Meng Y, Shen G, Schiferl D (2010) Structure of siderite FeCO<sub>3</sub> to 56 GPa and hysteresis of its spin-pairing transition. *Phys Rev B* 82:064110
- Le Bail A, Duroy H, Fourquet J (1988) Ab-initio structure determination of LiSbWO<sub>6</sub> by X-ray powder diffraction. *Mater Res Bull* 23:447–452
- Lin CC, Liu LG (1997a) High pressure phase transformations in aragonite-type carbonates. *Phys Chem Miner* 24:149–157
- Lin CC, Liu LG (1997b) High-pressure Raman spectroscopic study of post-aragonite phase transition in witherite (BaCO<sub>3</sub>). *Eur J Mineral* 9:785–792
- Lin JF, Liu J, Jacobs C, Prakapenka VB (2012) Vibrational and elastic properties of ferromagnesite across the electronic spin-pairing transition of iron. *Am Mineral* 97:583–591
- Litasov KD, Shatskiy A, Gavryushkin PN, Sharygin IS, Dorogokupets PI, Dymshits AM, Ohtani E, Higo Y, Funakoshi K (2013) P–V–T equation of state of siderite to 33 GPa and 1673 K. *Phys Earth Planet Inter* 224:83–87
- Liu LG, Lin CC (1997) A calcite → aragonite-type phase transition in CdCO<sub>3</sub>. *Am Mineral* 82:643–646
- Logvinova AM, Wirth R, Fedorova EN, Sobolev NV (2008) Nanometre-sized mineral and fluid inclusions in cloudy Siberian diamonds: new insights on diamond formation. *Eur J Mineral* 20:317–331
- Mao HK, Xu JA, Bell P (1986) Calibration of the ruby pressure gauge to 800 kbar under quasi-hydrostatic conditions. *J Geophys Res* 91:4673–4676
- Mao Z, Armentrout M, Rainey E, Manning CE, Dera P, Prakapenka VB, Kavner A (2011) Dolomite III: a new candidate lower mantle carbonate. *Geophys Res Lett* 38:L22303
- Martinez I, Zhang J, Reeder RJ (1996) In situ X-ray diffraction of aragonite and dolomite at high pressure and high temperature; evidence for dolomite breakdown to aragonite and magnesite. *Am Mineral* 81:611–624
- Mattei E, De Vivo G, De Santis A, Gaetani C, Pelosi C, Santamaria U (2008) Raman spectroscopic analysis of azurite blackening. *J Raman Spectrosc* 39:302–306
- Merlini M, Perchiazzi N, Hanfland M, Bossak A (2012) Phase transition at high pressure in Cu<sub>2</sub>CO<sub>3</sub>(OH)<sub>2</sub> related to the reduction of the Jahn–Teller effect. *Acta Cryst A* 68:266–274
- Minch R, Dubrovinsky L, Kurnosov A, Ehm L, Knorr K, Depmeier W (2010a) Raman spectroscopic study of PbCO<sub>3</sub> at high pressures and temperatures. *Phys Chem Miner* 37:45–56
- Minch R, Seoung DH, Ehm L, Winkler B, Knorr K, Peters L, Borkowski L, Parise J, Lee Y, Dubrovinsky L (2010b) High-pressure behavior of otavite (CdCO<sub>3</sub>). *J Alloys Compd* 50:251–257
- Nagai T, Ishido T, Seto Y, Nishio-Hamane D, Sata N, Fujino K (2010) Pressure-induced spin transition in FeCO<sub>3</sub>-siderite studied by X-ray diffraction measurements. *J Phys Conf Ser* 1:012002
- Oganov AR, Glass CW, Ono S (2006) High-pressure phases of CaCO<sub>3</sub>: crystal structure prediction and experiment. *Earth Planet Sci Lett* 241:95–103
- Oganov AR, Ono S, Ma Y, Glass CW, Garcia A (2008) Novel high-pressure structures of MgCO<sub>3</sub>, CaCO<sub>3</sub> and CO<sub>2</sub> and their role in Earth's lower mantle. *Earth Planet Sci Lett* 273:38–47

- Ohtani E (2006) The effect of water on mantle phase transitions. *Rev Miner Geochem* 62:397–420
- Ono S (2007a) High-pressure phase transformation in  $\text{MnCO}_3$ : a synchrotron XRD study. *Mineral Mag* 71:105–111
- Ono S (2007b) New high-pressure phases in  $\text{BaCO}_3$ . *Phys Chem Miner* 34:215–221
- Ono S, Kikegawa T, Ohishi Y, Tsuchiya J (2005) Post-aragonite phase transformation in  $\text{CaCO}_3$  at 40 GPa. *Am Mineral* 90:667–671
- Ono S, Kikegawa T, Ohishi Y (2007) High-pressure transition of  $\text{CaCO}_3$ . *Am Mineral* 92:1246–1249
- Ono S, Brodholt JP, Price GD (2008) Phase transitions of  $\text{BaCO}_3$  at high pressures. *Mineral Mag* 72:659–665
- Pavese A, Davide L, Pischetta V (2001) Elastic properties of andradite and grossular, by synchrotron X-ray diffraction at high pressure conditions. *Eur J Mineral* 13:929–937
- Pippinger T, Miletich R, Effenberger H, Hofer G, Lotti P, Merlini M (2014) High-pressure polymorphism and structural transitions of norsethite,  $\text{BaMg}(\text{CO}_3)_2$ . *Phys Chem Miner* 41:737–755
- Redfern SA (2000) Structural variations in carbonates. *Rev Mineral Geochem* 41:289–308
- Redfern SA, Angel RJ (1999) High-pressure behaviour and equation of state of calcite,  $\text{CaCO}_3$ . *Contrib Mineral Petrol* 134:102–106
- Ross NL (1997) The equation of state and high-pressure behavior of magnesite. *Am Mineral* 82:682–688
- Ross NL, Reeder RJ (1992) High-pressure structural study of dolomite and ankerite. *Am Mineral* 77:412–421
- Rule K, Reehuis M, Gibson M, Ouladdiaf B, Gutmann M, Hoffmann JU, Gerischer S, Tennant D, Süllo S, Lang M (2011) Magnetic and crystal structure of azurite  $\text{Cu}_3(\text{CO}_3)_2(\text{OH})_2$  as determined by neutron diffraction. *Phys Rev B* 83:104401
- Seto Y, Hamane D, Nagai T, Fujino K (2008) Fate of carbonates within oceanic plates subducted to the lower mantle, and a possible mechanism of diamond formation. *Phys Chem Miner* 35:223–229
- Shannon R (1976) Revised effective ionic radii and systematic studies of interatomic distances in halides and chalcogenides. *Acta Crystallogr* 32:751–767
- Skorodumova NV, Belonoshko AB, Huang L, Ahuja R, Johansson B (2005) Stability of the  $\text{MgCO}_3$  structures under lower mantle conditions. *Am Mineral* 90:1008–1011
- Smyth JR, Frost DJ, Nestola F (2005) Hydration of olivine and the Earth's deep water cycle. *Geochim Cosmochim Acta* 69:A746
- Stachel T, Harris JW, Brey GP, Joswig W (2000) Kankan diamonds (Guinea) II: lower mantle inclusion parageneses. *Contrib Mineral Petrol* 140:16–27
- Suito K, Namba J, Horikawa T, Taniguchi Y, Sakurai N, Kobayashi M, Onodera A, Shimomura O, Kikegawa T (2001) Phase relations of  $\text{CaCO}_3$  at high pressure and high temperature. *Am Mineral* 86:997–1002
- Townsend JP, Chang Y-Y, Lou X, Merino M, Kirklin SJ, Doak JW, Issa A, Wolverton C, Tkachev SN, Dera P, Jacobsen SD (2013) Stability and equation of state of post-aragonite  $\text{BaCO}_3$ . *Phys Chem Miner* 40:447–453
- Wang A, Pasteris JD, Meyer HO, Dele-Duboi ML (1996) Magnesite-bearing inclusion assemblage in natural diamond. *Earth Planet Sci Lett* 141:293–306
- Xu J, Ma M, Wei S, Hu X, Liu J, Liu J, Fan D, Xie H (2014) Equation of state of adamite up to 11 GPa: a synchrotron X-ray diffraction study. *Phys Chem Miner* 41:547–554
- Zha CS, Duffy TS, Downs RT, Mao HK, Hemley RJ (1998) Brillouin scattering and X-ray diffraction of San Carlos olivine: direct pressure determination to 32 GPa. *Earth Planet Sci Lett* 159:25–33
- Zhang J, Reeder RJ (1999) Comparative compressibilities of calcite-structure carbonates: deviations from empirical relations. *Am Mineral* 84:861–870
- Zhang YF, Liu J, Qin ZX, Lin CL, Xiong L, Li R, Bai LG (2013) A high-pressure study of  $\text{PbCO}_3$  by XRD and Raman spectroscopy. *Chin Phys C* 37:1–5
- Zigan F, Schuster HD (1972) Refinement of azurite structure,  $\text{Cu}_3(\text{OH})_2(\text{CO}_3)_2$  by neutron diffraction. *Z Kristallogr Kristallgeom Kristallphys Kristallchem* 135:416–436